44. Optical Nonlinearity in Photonic Glasses

A brief review of optical nonlinearity in photonic glasses is given. For third-order nonlinearity, the relationship between two-photon absorption and nonlinear refractive index is considered using a formalism developed for crystalline semiconductors. Stimulated light scattering and supercontinuum generation in optical fibers are also introduced. Prominent resonant-type nonlinearity in particle-embedded glasses is described. For second-order nonlinearity, a variety of poling methods are summarized. Finally, it is pointed out that various photoinduced changes can appear when excited by linear and nonlinear optical processes, and this is related to glass structure.

New developments in optical fibers and pulsed lasers have prompted increasing interest in optical nonlinearity in photonic glasses [44.1–3]. Third-order polarization yields several nonlinear phenomena, such as intensity-dependent absorption and intensity-dependent refractive index, which can be utilized in power stabilizers and all-optical switches. On the other hand, in high-power glass lasers, self-focusing effects arising from intensity-dependent increases in refractive index pose serious problems. Then again, the second-order polarization that occurs in poled glasses can be utilized in second harmonic generation for example. The present chapter provides a brief review of optical nonlinearity in *inorganic* glasses. At this point we should mention that, in many respects, organic polymers exhibit similar features to those of glass [44.4, 5]. In general, glass is more stable, while polymers can provide greater nonlinearity, so these two types of material are competitors in practical applications.

Glass also competes with crystals. A great advantage of glass is the ability to control its structure at three scales. First, the atomic composition of the glass can be tailored continuously. For instance, we can obtain nonlinear optical glass with any refractive index in the range of 1.4–3.2 at a wavelength of $\approx 1\,\mu\mathrm{m}$. Second, the atomic structure can be modified reasonably easily using, e.g., light beams. Such modifications may be regarded as photoinduced phenomena, which can be employed in order to add second-order nonlinearity to selected regions and so forth. Lastly, macroscopic shapes can be changed into arbitrary bulk forms, fibers, thin layers and microparticles [44.6, 7].

Here, fiber and film waveguides may be very important for nonlinear applications for two reasons. One is that the light power density can be increased by reducing the lateral size, i. e. the film thickness or fiber diameter, to submicron scales. The other is, that fibers can provide long lengths for light–glass interactions that are not limited by diffraction. These scale factors produce apparent enhancements in nonlinear effects in glasses, although the intrinsic nonlinearity may be smaller than that in crystals.

Before proceeding further, it would be useful to introduce a nonlinear formula [44.4, 5]. For simplicity, we take the polarization P and the electric field E to be scalar quantities. Then, very simply, P can be written down in the cgs units as

$$P = \chi^{(1)}E + \chi^{(2)}EE + \chi^{(3)}EEE + \ldots , \qquad (44.1)$$

where the first term $\chi^{(1)}E$ depicts the conventional linear response, and $\chi^{(2)}$ and $\chi^{(3)}$ represent the second- and the third-order nonlinear susceptibilities. $\chi^{(1)}$ is related to the linear refractive index n_0 via $n_0 = \left\{1 + 4\pi\chi^{(1)}\right\}^{1/2}$. On the other hand, the second term provides such time dependence as $\sin\{(\omega \pm 2\omega)t\}$, so that it could produce dc and second-overtone (2ω) signals. In a similar way, the

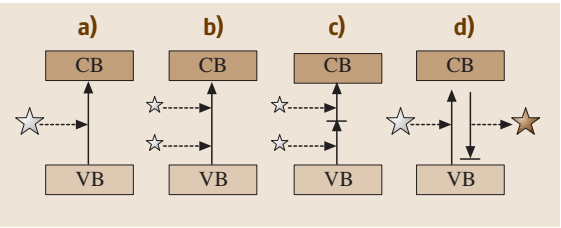

Fig. 44.1a–d Schematic illustrations of **(a)** one-photon absorption, **(b)** two-photon absorption, **(c)** two-step absorption via a mid-gap state, and **(d)** a Raman-scattering process in a semiconductor with a valence band (VB) and a conduction band (CB)

third could modify the fundamental (ω) signal and generate a third-overtone (3ω). Nevertheless, since a refractive index changes with frequency, it is difficult in the overtone generations to satisfy the so-called phase-matching condition [44.4,5], e.g. $\varphi_{3\omega} = 3\varphi_{\omega}$, where φ is the phase of electric fields in glasses. The, the fundamental-signal processing may be the most important. Microscopically, the nonlinear terms arise through several mechanisms, such as electronic, atomic (including molecular motions), electrostatic and thermal processes. Among these, electronic processes can provide the fastest responses, with fs–ps time scales, which will be needed for optical information technologies. Accordingly, we will focus on such processes from this point onwards.

The chapter is divided up as follows. In Sect. 44.1, we treat conventional glasses. These are optically isotropic, which gives $\chi^{(2)} = 0$, because the isotropic structure appears to be centrosymmetric. In this case, the lowest nonlinear term becomes $\chi^{(3)}EEE$. When $\chi^{(3)}EEE$ can be written as $\chi^{(3)}IE$, where I is the light intensity, we can define the refractive index n as $n = n_0 + n_2 I$, where n_2 is sometimes called the second-order index of refraction [44.5]. In nonlinear optics, this notation poses problems due to the definitions of several parameters. Therefore, the conversion $n_2(\mathrm{cm}^2/\mathrm{W}) \approx 0.04\chi^{(3)}(\mathrm{esu})/n_0^2$ is frequently employed [44.5]. On the other hand, for light absorption, which is proportional to $\langle E\,\mathrm{d}P/\mathrm{d}t\rangle$, where $\langle \ldots \rangle$ represents a time average, we need to take the imaginary parts of $\chi^{(1)}$ and $\chi^{(3)}$, which cause one- and two-photon absorption, into account (Fig. 44.1). In such cases, an effective absorption coefficient can be written as $\alpha(\mathrm{cm}^{-1}) + \beta(\mathrm{cm/W})I(\mathrm{W/cm}^2)$; n_2 and β will be connected through nonlinear Kramers–Kronig relations.

Section 44.2 focuses upon noncentrosymmetry. From the mid-1980s onwards, several kinds of poling treatments have been found to add $\chi^{(2)}$ to glasses [44.8]. For instance, *Österberg* and *Margulis* [44.9] demonstrated intense second harmonic generation in laser-irradiated glass fibers. Such work began with silica, and has more recently been directed towards more complicated glasses. The magnitude of $\chi^{(2)}$ seen in this case may be smaller than those observed in crystals, due to the disordered atomic structures in glasses, but the structural controllability may offer some advantages.

Section 44.3 introduces glasses incorporating fine semiconductor and metal particles. Such nanostructured glasses are known to exhibit large optical nonlinearities [44.4, 5, 10]. However, as will be described, their wider features remain to be studied.

In Sect. 44.4 we consider photoinduced phenomena. The intense light needed to produce optical nonlinearity is likely to modify the structure of glass. Light that is even more intense may cause damage. While this damage can be useful for optical engraving, the structural modification may ultimately be more important. Actually, fiber Bragg gratings [44.1, 11] have been produced commercially using excimer lasers, and nonlinear optical excitation may play an important role in these. Three-dimensional modifications are also produced through controlled light focusing [44.12]. Section 44.5 provides a summary of the chapter. This chapter is based on author's recent review [44.13].

44.1 Third-Order Nonlinearity in Homogeneous Glass

44.1.1 Experimental

Substantial data are available for n_2 at transparent wavelengths [44.4]. However, to the author's knowledge, all such experiments have utilized lasers, and no spectral dependence has been reported. We should also note that, in comparison with n_0 measurements, n_2 evaluations are much more difficult [44.4]. The biggest difficulty, which is common to all nonlinear experiments, is the light intensity. Normally, light is pulsed and focused, producing complex temporal and spatial profiles, which in turn means that intensity evaluations are not straightforward. For instance, if the profile is Gaussian, can we simply use the peak value to evaluate the nonlinearity? Because of such measuring difficulties and also some other specific problems inherent to

Table 44.1 Linear (E_g, n_0, α_0) and nonlinear (n_2, β, β_{max}) optical properties and figures of merit ($2\beta\lambda_0/n_2$, n_2/α_0) in some glasses. E_g is the optical bandgap energy [44.12], n_0 is the refractive index [44.12], α_0 is the attenuation coefficient [44.16], n_2 is the intensity-dependent refractive index [44.4,5,12], β is the two-photon absorption coefficient [44.16], and β_{max} is the maximum value. Except for E_g and β_{max}, the values are evaluated at a wavelength of 1–1.5 μm. BK-7 is a borosilicate glass and SF-59 indicates data for lead-silicate glasses with ≈ 57mol.% PbO

Glass	E_g (eV)	n_0	α_0 (cm^{-1})	n_2 (10^{-20} m^2/W)	β (cm/GW)	β_{max} (cm/GW)	$2\beta\lambda_0/n_2$	n_2/α_0 (cm^3/GW)
SiO_2	10	1.5	10^{-6}	2	$< 10^{-2}$	1	< 10	0.2
BK-7	4	1.5		3				
SF-59	3.8	2.0		30	$< 10^{-1}$	10		
As_2S_3	2.4	2.5	10^{-3}	200	10^{-2}	50	0.1	0.02
BeF_2	10	1.3		0.8				

glasses, reported n_2 values vary, even for a reference SiO_2 glass, over the range $1–3\times10^{-20}$ m^2/W [44.4]. In other glasses, values that differ by a factor of ≈ 10 have been reported [44.4, 14, 15].

However, we can see a general trend in n_2 in Table 44.1. Halide glasses (BeF_2) have the smallest values, light metal oxides (BK-7) and SiO_2 have similar values, heavy metal oxides such as PbO-SiO_2 (SF-59) have larger values, while the largest belong to the chalcogenides (As_2S_3) [44.4, 10]. The largest value reported so far may be $n_2 = 8\times10^{-16}$ m^2/W, seen in $Ag_{20}As_{32}Se_{48}$ at wavelength of 1.05 μm [44.21], which is ≈ 10^4 times as large as that of SiO_2.

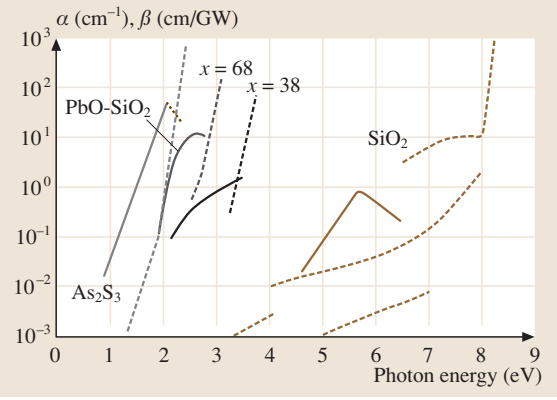

Fig. 44.2 One- (*dashed line*) and two-photon (*solid line*) absorption spectra, α and β, in SiO_2 [44.17, 18], 38PbO – 62SiO_2, 68PbO – 32SiO_2 [44.19], and As_2S_3 [44.20]. For SiO_2, in transparent regions ($\hbar\omega \leq 8.0$ eV) α should be regarded as an attenuation coefficient; these are not reproducible, probably due to impurities, defects and light scattering. The *dotted line* for As_2S_3 at $\hbar\omega \geq 2.0$ eV indicates two-step absorption

Figure 44.2 shows β spectra for SiO_2, As_2S_3 and two PbO-SiO_2 glasses [44.16]. Bi_2O_3-B_2O_3 glasses (*Imanishi* et al., [44.22]) exhibit similar features to those of lead glass. We can see that all of the β spectra seem to have maxima at midgap regions, $\hbar\omega \approx E_g/2$. However, this is not an absolute rule, since at $\hbar\omega \geq 2.0$ eV As_2S_3 provides two-step absorption (Fig. 44.1), which masks the two-photon absorption signal [44.20]. We also see that the maximal β (≈ 10^0 cm/GW) in SiO_2 is markedly smaller than those belonging to the other glasses. Note that such a marked difference does not exist in maximal α, which is ≈ 10^6 cm^{-1} at the super-bandgap regions of SiO_2 and As_2S_3. It may be worth mentioning here that two-photon excitation produces photocurrents in some glasses [44.23, 24].

44.1.2 Theoretical Treatment

For $\chi^{(3)}$, theoretical treatments of glasses, liquids, and crystals are largely the same. Glasses and liquids can be treated similarly in the sense that both are optically isotropic. Hence, many ideas stemming from types of chemical bond pictures have been proposed [44.5]. On the other hand, the magnitude of $\chi^{(3)}$ in glass appears to be similar to that in the corresponding crystal, since their electronic structures are both governed by short-range atomic structures, within ≈ 0.5 nm [44.25], which is much shorter than the wavelength (≈ 500 nm) of visible light. Specifically, since n_2 is governed by integrated electronic absorption (44.8), the magnitudes are roughly the same in glass and crystal. For instance, in crystalline and glassy SiO_2 at near-infrared wavelengths, the difference in the n_2 values of both seems to be comparable with their experimental accuracy; i. e. the values for crystalline and glassy SiO_2 are ≈ 1.14×10^{-13} and 0.85×10^{-13} esu respectively [44.4]. Then, using a formula derived for semiconductor crystals, we can apply

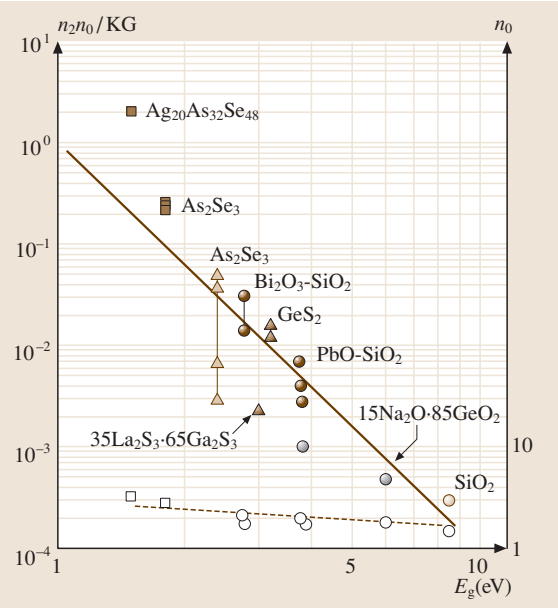

Fig. 44.3 The Sheik–Bahae relation $n_2 n_0 = KG(\hbar\omega/E_g)/E_g^4$ (*solid line*), related data (*solid symbols*), the Moss rule $n_0^4 E_g = 77$ (*dashed line*), and related data (*open symbols*) for an oxide (*circles*), sulfide (*triangles*) and selenide (*squares*). The four data for As_2S_3 are obtained from different publications, while those for PbO-SiO_2 with slightly different E_g correspond to different compositions. The illustration is modified from its previous form [44.16] due to the additions of $Ag_{20}As_{32}Se_{48}$ [44.21], Bi_2O_3-silica glasses [44.26], $35La_2S_3 - 65Ga_2S_3$ [44.27], and $15Na_2O - 85GeO_2$ [44.28]

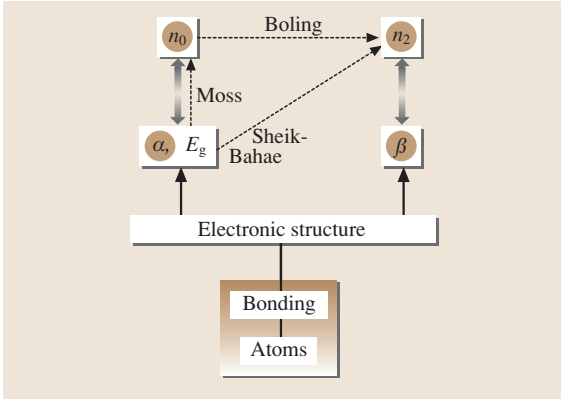

Fig. 44.4 Relationship between atomic structure, electronic structure, linear absorption α including bandgap energy E_g, linear refractive index n_0, two-photon absorption β, and nonlinear refractive index n_2. Absorption and refraction are related by the linear and nonlinear Kramers–Kronig relations (*double arrows*). The Moss rule may be regarded as a simplified Kramers–Kronig relation. The Boling and Sheik–Bahae relations connect n_0 and E_g to n_2, respectively

a kind of band picture to glasses [44.16], as described below.

Estimation of Nonlinear Refractivity

Several semi-empirical relationships have been proposed for $\chi^{(3)}$ or n_2 [44.5]. Such relations are useful, since nonlinear optical constants are much more difficult to measure than linear constants. Naturally, since they are simplifications they are also less accurate. The simplest may be the one provided by *Wang*, $\chi^{(3)} \approx \{\chi^{(1)}\}^4$, which can be regarded as a generalized Miller's rule [44.5]. *Boling* et al. [44.29] have also derived some relations, among which the simplest may be

$$n_2(10^{-13}\,\text{esu}) \approx 391(n_d - 1)/\nu_d^{5/4}\,, \qquad (44.2)$$

where n_d is the refractive index at the d-line ($\lambda = 588\,\text{nm}$) and ν_d is the Abbe number. This relation contains only two macroscopic parameters, which can be easily evaluated, and so it has often been used to estimate n_2. It actually provides a good approximation for small n_d glasses with $n_d \le 1.7$ [44.29]. For high n_d glasses, *Lines* [44.14] proposes a relation that also contains the atomic distance, and others derive more complicated formula [44.30, 31]. Ab initio calculations for TeO_2-based glasses have also been reported recently [44.32]. However, these relations cannot predict wavelength dependence (Fig. 44.5). The estimated n_2 may be regarded as a long-wavelength limit. In addition, the material is regarded as transparent, so relations between n_2 and β cannot be found.

Nonlinear optical properties of semiconductor crystals have been studied fairly deeply [44.5], and applying the same concepts to glasses appears to be tempting. *Tanaka* [44.16] has adopted a band picture, which was developed by *Sheik-Bahae* et al. [44.33], to some glasses. Their concept gives a universal relationship of

$$n_2 = KG(\hbar\omega/E_g)/(n_0 E_g^4)\,, \qquad (44.3)$$

for crystals with energy gaps of 1–10 eV, where K is a fixed constant and $G(\hbar\omega/E_g)$ is a spectral function (E_g is the bandgap energy). For E_g in glasses, we can take the so-called Tauc gap [44.25] if it is known, or otherwise the photon energy $\hbar\omega$ at $\alpha \approx 10^3\,\text{cm}^{-1}$. As shown in Fig. 44.3, the universal line gives reasonable agreement with published data, while the agreement is

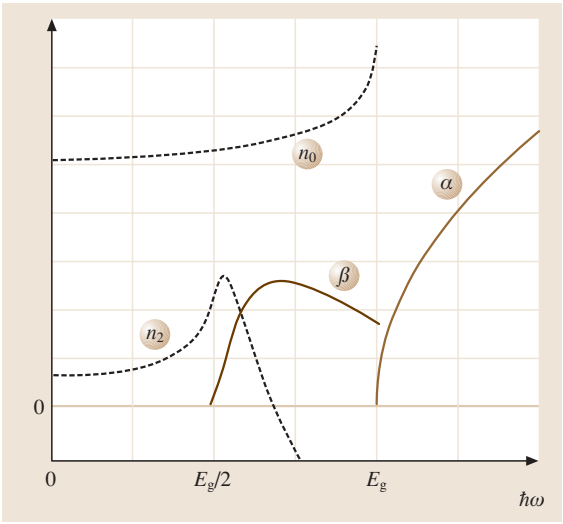

Fig. 44.5 Spectral dependence of linear absorption α, linear refractive index n_0, two-photon absorption β, and intensity-dependent refractive index n_2 in an ideal amorphous semiconductor with energy gap E_g. *Vertical scales* are arbitrary

not satisfactory as it is for crystals [44.33]. The poorer agreement for glasses may be partly due to experimental difficulties. In addition, band tail states probably cause larger deviations in smaller bandgap glasses such as $Ag_{20}As_{32}Se_{48}$. Incidentally, as shown by the dashed line in the figure, the Moss rule $n_0^4 E_g = 77$ [44.34], which was originally pointed out for crystalline semiconductors, also gives satisfactory fits for glasses.

Nonlinear Kramers–Kronig Relationship

We can take another approach in order to obtain unified insight into optical nonlinearity (n_2 and β). In this case, we start with absorption and then obtain the refractive index using Kramers–Kronig relationships. As illustrated in Fig. 44.4, this approach is able to provide a complete understanding of atomic structure and optical properties, since absorption spectra can be related to electronic structure more directly.

It is well-known that, for glasses, and neglecting momentum conservation rules, $\alpha(\hbar\omega)$ and $\beta(\hbar\omega)$ can be written as [44.16]

$$\alpha(\hbar\omega) \propto |\langle\phi_f|H|\phi_i\rangle|^2 \int D_f(E+\hbar\omega) D_i(E)\,\mathrm{d}E\,, \tag{44.4}$$

$$\beta(\hbar\omega) \propto |\Sigma_n \langle\phi_f|H|\phi_n\rangle\langle\phi_n|H|\phi_i\rangle/(E_{ni}-\hbar\omega)|^2 \times \int D_f(E+2\hbar\omega) D_i(E)\,\mathrm{d}E\,, \tag{44.5}$$

where H is the perturbation Hamiltonian, ϕ is a related electron wavefunction, and D is the density of states, and the subscripts i, n, and f represent the initial, intermediate, and final states. α and β are linked to the electronic structure, i. e. the wavefunctions and densities of states, which is determined by the atomic species and bonding structures involved [44.25]. In this case, $n_0(\omega)$ is expressed using the conventional Kramers–Kronig relation as [44.5]

$$n_0(\omega) = 1 + (c/\pi)\wp \int \left[\alpha(\Omega)/(\Omega^2-\omega^2)\right]\mathrm{d}\Omega\,. \tag{44.6}$$

For a nonlinear response Δn, *Hutchings* et al. [44.35] have derived the relation

$$\Delta n(\omega;\zeta) = (c/\pi)\wp \int \left[\Delta\alpha(\Omega;\zeta)/(\Omega^2-\omega^2)\right]\mathrm{d}\Omega\,, \tag{44.7}$$

where $\Delta\alpha$ is the nonlinear absorption induced by an excitation at ζ and probed at Ω. Note that this relation is derived from the causality principle for nondegenerate cases, e.g., two-beam experiments with different photon energies, Ω and ζ. However, this relation may also be applied to degenerate cases ($\Omega = \zeta$) as a rough approximation as [44.36]

$$n_2(\omega) = (c/\pi)\wp \int \left[\beta(\Omega)/(\Omega^2-\omega^2)\right]\mathrm{d}\Omega\,. \tag{44.8}$$

Using these formulae, we can roughly predict how β and n_2 depend upon E_g. Equation (44.5) suggests that $\beta \propto 1/E_g^2$, provided that the E_g dependence is governed by $|\Sigma_n 1/(E_{ni}-\hbar\omega)|^2$. This relation may be consistent with the material dependence shown in Fig. 44.2. That is, $\beta_{max} \propto 1/E_g^2 \approx 1/E_g^3$. Note that this E_g dependence is comparable to $\beta \propto 1/E_g^3$, which is theoretically derived and experimentally confirmed for crystalline semiconductors [44.5, 33]. Then, putting $\beta \propto 1/E_g^2$ into (44.8), and assuming $\int[1/(\Omega^2-\omega^2)]\mathrm{d}\Omega \propto 1/E_g^2$, we obtain $n_2 \propto 1/E_g^4$, which is consistent with (44.3).

Under some plausible assumptions, we can also calculate the spectral dependence of β and n_2 for an ideal amorphous semiconductor, which contains no gap states [44.37]. Figure 44.5 shows that, at $\hbar\omega = E_g/2$, $\beta = 0$ and n_2 is maximal. This is similar to some degree to the feature at $\hbar\omega = E_g$ for α and n_0. The figure also shows that β becomes maximal at $E_g/2 - E_g$. Note, however, that it is not clear whether we can link this photon energy dependence to the experimental results shown in Fig. 44.2, since the observed spectra appear to have fairly sharp peaks.

Figure of Merit

Several figures of merit have been proposed for evaluating optical devices which utilize n_2. For instance, *Mizrahi* et al. [44.40] and others [44.15, 21, 41] emphasize the negative effects of two-photon absorption, and provide the criterion that $2\beta\lambda_0/n_2 < 1$. Then, using the above E_g dependence, we see that $\beta/n_2 \approx E_g^2$, so that small E_g materials are preferable. Actually (as also listed in Table 44.1), in this figure, As_2S_3 appears to be better than SiO_2. However, the criterion implicitly neglects α. *Lines* [44.14] uses n_2/α instead. Here, α arises from the so-called residual absorption, which is difficult to estimate quantitatively. In addition, it is the attenuation α_0 instead of the absorption α that could be decisive. Table 44.1 shows that, in this measure, SiO_2 behaves better than As_2S_3. These figures of merit, however, have presumed only nonresonant electronic contributions with sub-ps responses. More recently, *Jha* et al. [44.10] utilize $n_2/\tau\alpha$, where τ is the relaxation time. Nevertheless, theoretical predictions of τ remain to be studied.

The most appropriate definition of the figure of merit naturally depends upon the application of interest. For instance, for an optical fiber device, the maximum length might be ≈ 1 m [44.42], since the device must be compact and fast. In this case, the light absorption, which arises from $\alpha + \beta I$, should be suppressed to below $10^{-2}\,\mathrm{cm}^{-1}$, or the light propagation loss must be smaller than ≈ 1 dB/m. However, for optical integrated circuits, an effective propagation distance may be ≈ 1 cm, in which the attenuation could be as large as $10^{0}\,\mathrm{cm}^{-1}$.

We can suggest another idea by taking the spectral dependence shown in Fig. 44.5 into account. That is, the best material that has n_2 at some $\hbar\omega$ is the one which satisfies a bandgap condition of $\hbar\omega = E_g/2$, where α and β are zero and n_2 becomes maximal, provided that there is no gap-state absorption. In practical glass samples, absorption due to impurities, dangling bonds such as E' centers in oxide glasses [44.11, 25], and wrong bonds in chalcogenide glasses [44.25, 37] cannot be neglected. Actually, we can see in Table 44.1 and Fig. 44.2 that residual attenuation exists in nominally transparent regions, parts of which are undoubtedly caused by absorption [44.43]. Note that these mid-gap states also give rise to two-step absorption (Fig. 44.1). We also cannot neglect photoinduced phenomena induced by these photoelectronic excitations (Sect. 44.4). Selecting an appropriate glass for a specific application is, therefore, not a straightforward process.

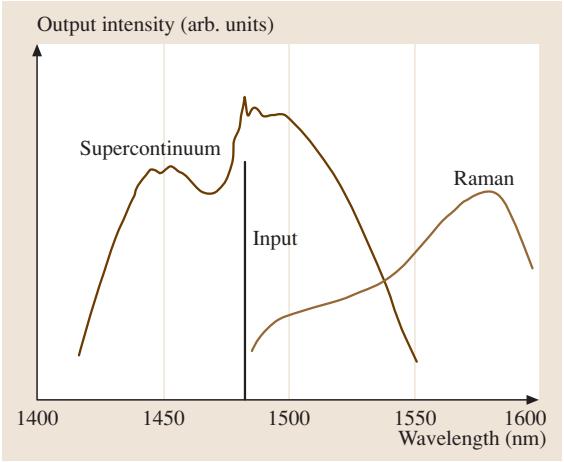

Fig. 44.6 Output spectra from a Raman fiber amplifier [44.38] and from a supercontinuum fiber generator [44.39] excited by 1483 nm light (schematic illustration)

44.1.3 Stimulated Light Scattering and Supercontinuum Generation

Recently, stimulated Raman scattering has attracted considerable interest, since it can be utilized for broadband light amplification [44.1, 5]. As illustrated in Fig. 44.1d, stimulated Raman scattering can be regarded as a kind of nondegenerate two-photon process. However, in contrast to two-photon absorption, one photon is absorbed by a virtual state at the same time as another photon is emitted in Raman scattering. As with conventional stimulated light emission, when the incident light is intense, the Stokes-shifted light can be amplified. The nonlinear polarization related to this is given by $P^{(3)}(\omega_s) \propto i\chi_R^{(3)} I(\omega_L) E(\omega_s)$, or the emitted light intensity is $\Delta I(\omega_s) \propto \chi_R^{(3)} I(\omega_L) I(\omega_s)$, where ω_L and $\omega_s (< \omega_L)$ are the exciting laser frequency and the Stokes-shifted frequency.

Most experiments have been performed using optical fibers [44.1, 42] in order to obtain long interaction lengths. For instance, as illustrated in Fig. 44.6, Raman fiber amplifiers comprising 5–10 km lengths of silica can provide broadband gains of ≈ 10 dB [44.38]. Raman lasers using silica microspheres of diameter $\approx 70\,\mu$m [44.7] are also interesting examples. On the other hand, stimulated Brillouin scattering in glasses has also been explored [44.1, 4].

Supercontinuum generation in silica fibers has now been studied intensively [44.4, 39, 44]. When pulsed or CW light propagates through a nonlinear medium, it may undergo spectral broadening [44.5].

For instance, as illustrated in Fig. 44.6, a 350 m single-mode fiber excited by a 2.22 W CW laser with a wavelength of 1.483 μm can emit 2.1 W over a broad spectrum of 1.43–1.53 μm [44.39]. Note that, unlike the stimulated light scattering described above, light of a shorter wavelength is also generated in this process. Such a spectral-conversion fiber could be utilized as a broadband optical amplifier. The phenomenon appears under strong and prolonged nonlinear interactions, and accordingly, several mechanisms such as intensity-dependent refractive index changes, third harmonic generation and stimulated Raman scattering could be responsible [44.39].

44.2 Second-Order Nonlinearity in Poled Glass

It has been discovered that several kinds of poling methods can add second-order nonlinearity to glasses [44.8]. At least five kinds have been demonstrated, which are listed in Table 44.2. Note that similar procedures are also employed for polymers. Most experiments utilize second harmonic signals to evaluate $\chi^{(2)}$ and, less commonly, electro-optical effects. Practical applications remain to be studied, while, for second-harmonic generations, the optical phase matching between exciting and nonlinearly-generated light is a prerequisite [44.45].

This so-called optical poling was demonstrated by *Österberg* and *Margulis* [44.9] using optical fibers. They found that exposing Ge-doped optical fibers of length ≈ 1 m to 70 kW Nd:YAG laser light for ≈ 1 h could increase the second-harmonic signal to 0.55 kW. *Stolen* and *Tom* [44.46] utilized two light beams (x1 and x2, of Nd:YAG laser light) for induction, which reduced the exposure time to ≈ 5 min. However, the method was only practical for optical fibers, since the nonlinearity induced was relatively small, $\chi^{(2)} \approx 10^{-4}$ pm/V. Second, so-called thermal poling, which was actually electrothermal in nature, was demonstrated in *bulk* SiO_2 samples by *Myers* et al. [44.47]. The nonlinearity induced, ≈ 1 pm/V, which was evaluated from the second harmonic signals of 1.06 μm laser light, is of a similar magnitude to that in quartz. Since this nonlinearity is reasonably large, this method has been widely applied to other glasses, such as PbO-SiO_2 [44.48], Nb_2O_5-B_2O_3-P_2O_5-CaO [44.49], and TeO_2-Bi_2O_3-ZnO [44.50]. Third, *Okada* et al. [44.51] demonstrated the corona-discharge poling at ≈ 200 °C of 7059 *films* deposited onto Pyrex glass substrates. This corona-poling procedure has often been employed for organic polymers. Fourth, electron-beam poling of PbO-silica glass was shown to produce ≈ 1 pm/V [44.52]. An advantage of this method is its high resolution, which may hold promise in the fabrication of optical integrated circuits, despite the fact that a vacuum is needed. *Liu* et al. (2001) [44.53] applied the method to chalcogenide glasses, which produced ≈ 1 pm/V. Proton implantation into silica can also add a $\chi^{(2)}$ of ≈ 1 pm/V [44.54]. Sixth, *Fujiwara* et al. (1997) demonstrated UV poling in Ge-doped SiO_2 subjected to electric fields of $\approx 10^5$ V/cm. The $\chi^{(2)}$ induced is reported to be ≈ 3 pm/V, comparable to that in $LiNbO_3$.

Table 44.2 Reported poling methods, applied objects, typical procedures, and induced $\chi^{(2)}$ values in silica. For references, see the main text. The $\chi^{(2)}$ values listed are compared with $\chi^{(2)}_{11} = 1$ pm/V in crystalline SiO_2 and $\chi^{(2)}_{22} = 5$ pm/V in $LiNbO_3$

Method	Object	Procedure	$\chi^{(2)}$ (pm/V)
Optical	Fiber	Nd:YAG laser, 1 h	10^{-4}
Thermal	Bulk	4 kV, 300 °C, 1 h	1
Corona	Film	5 kV, 300 °C, 15 min	1
e-beam	Bulk	40 kV, 10 mA, 10 min	1
Proton	Bulk	500 kV, 1 mC, 100 s	1
UV	Bulk	ArF laser, 10 kV	3

Two poling mechanisms of note have been proposed [44.8]. One is that space charge produces a built-in electric field of E_{DC} ($\approx 10^6$ V/cm), which induces an effective $\chi^{(2)}$ of $3E_{DC}\chi^{(3)}$ [44.46]. Here, E_{DC} is governed by the migration of ions such as Na^+ under applied or generated electric fields [44.55]. In agreement with this idea, $\chi^{(2)}$ decays with a time constant of 10^1–10^6 days at room temperature, which is connected to the alkali ion mobility [44.55]. The other idea is that oriented defects such as E' centers are responsible. It is reasonable to assume that UV excitation produces defective dipoles, which are oriented with the static electric field.

It may be reasonable to assume that the dominant mechanism depends upon the poling method. Actually, we can divide the procedures listed in Table 44.2 into two types, depending upon whether or not the glass is heated during the poling process. The heating tends to enhance macroscopic ion migration,

while it can also relax microscopic defect orientations at the same time [44.25]. Therefore, it seems that the ion migration is responsible in thermal and coronal poling, while defect orientation dominates in the other methods. In this context, poling at low temperatures may be a promising way of enhancing defect orientation.

In so-called *glass ceramics*, embedded crystals seem to be responsible for prominent $\chi^{(2)}$ [44.50, 56, 57]. For instance, *Takahashi* et al. [44.57] demonstrated that oriented $Ba_2TiSi_2O_8$ crystals are produced in BaO-TiO_2-SiO_2 glass by heat treatment at 760 °C for 1 h, which gives a prominent $\chi^{(2)}$ of ≈ 10 pm/V. $\chi^{(2)}$ can also be generated at interfaces [44.58].

44.3 Particle-Embedded Systems

Glasses that contain nanoparticles of metals [44.65, 66] and semiconductors [44.67] have attracted considerable interest due to their unique third-order nonlinearities. Table 44.3 lists several recent results. Such glasses containing dispersed nanoparticles can be prepared by a variety of physical and chemical methods, e.g., vacuum deposition and sol-gel techniques [44.4, 65, 68]. For semiconductor systems, a lot of work has also been investigated in semiconductor-doped color glass filters [44.67], which are now commercially available.

These nanoparticle systems work efficiently at close to the resonant wavelengths of some electronic excitations. This feature produces at least three characteristics. First, the imaginary, not the real, part of $\chi^{(3)}$ may be more prominent. Accordingly, Table 44.3 compares absolute values. Second, the system exhibits a strong spectral dependence [44.4, 69]. For instance, Au-silica and CdSSe-silica are efficient at ≈ 580 nm and ≈ 800 nm [44.4]. Third, the response time τ and the linear absorption α tend to become longer and higher. Actually, a trade-off between $\chi^{(3)}$ and τ and α seems to exist. For instance, CdSSe-dispersed glasses show $\chi^{(3)}$ value of $\approx 10^{-9}$ esu with τ value of ≈ 20 ps, while Au-dispersed glasses give $\approx 10^{-11}$ esu and ≈ 1 ps, respectively [44.4]. Linear absorption can be as large as 10^4 cm^{-1} [44.65], so these systems can be utilized as small devices, not as fibers. Note that, in pure silica at nonresonant infrared wavelengths, $\chi^{(3)} \approx 10^{-13}$ esu, $\tau \approx 10$ fs, and $\alpha \leq 10^{-5}$ cm^{-1} [44.65]. As is suggested above, the particle-embedded system should surmount two problems for wide applications. One is the reduction of linear attenuation, including absorption and scattering, and the other is the shift of resonant wavelengths to the optical communication region, 1.3–1.5 μm. Is such a shift possible? What are the mechanisms that give rise to these prominent nonlinearities in particle-embedded systems?

When the particle is a semiconductor such as CuCl and CdSSe, excitons or confined electron-hole pairs are responsible [44.67]. Specifically, the excitons in semiconductor particles behave as two-level systems, and at the resonance frequency, $|\chi^{(3)}|$ is written as

$$|\chi^{(3)}| \approx \mathrm{Im}\chi^{(3)} \propto |\mu|^4 N T_1 T_2^2 \,, \qquad (44.9)$$

where μ is the dipole moment of the exciton, N is the particle number, $T_1 (\approx 100$ ps) is the lifetime of the exciton, and $T_2 (\approx$ fs) is the dephasing time. A quantitative estimation predicts that closely packed CuCl particles of radius 40 nm could provide a $|\chi^{(3)}|$ enhancement of a factor of $\approx 10^3$ when compared with the bulk value [44.70].

When metal particles such as spherical Au particles with diameters of 10–50 nm are used, we can envisage

Table 44.3 Several recently reported particle systems, along with their preparation methods, $|\chi^{(3)}|$ values, and response times τ at the measured wavelength λ, as well as references. PLD and VE depict pulsed laser deposition and vacuum evaporation

System	Preparation	$\lvert\chi^{(3)}\rvert$ (esu)	τ	λ (nm)	Reference
Au (15 nm)/ silica	Shell structure	10^{-9}	2 ps	550	[44.59]
Cu (2 nm)/Al_2O_3	PLD	10^{-7}	5–450 ps	600	[44.60]
Ag (20 nm)/BaO	VE	10^{-10}	0.2 ps	820	[44.61]
Fe (4 nm)/$BaTiO_3$	PLD	10^{-6}		532	[44.62]
SnO_2 (10 nm)/silica	Sol-gel	10^{-12}		1064	[44.63]
CdS (4 nm)/silica	Sol-gel	10^{-11}		500	[44.64]

local field enhancement and dynamic responses from conduction electrons, including plasmon effects [44.65, 66, 71]. The result is approximately written as

$$\chi^{(3)} \approx p_{\mathrm{m}} \chi_{\mathrm{m}}^{(3)} |3\varepsilon_{\mathrm{h}}/(\varepsilon_{\mathrm{m}} + 2\varepsilon_{\mathrm{h}})|^2 \{3\varepsilon_{\mathrm{h}}/(\varepsilon_{\mathrm{m}} + 2\varepsilon_{\mathrm{h}})\}^2 , \quad (44.10)$$

where p_{m} is the volume fraction of the metal particles, $\chi_{\mathrm{m}}^{(3)}$ is the bulk nonlinearity of the metal, and ε_{h} and ε_{m} are the linear dielectric constants of the host (glass) and the metal. The nonlinearity of the host is neglected here for the sake of simplicity. Note that ε_{h} can be real, while ε_{m} is complex. We see that the metal's nonlinearity $\chi_{\mathrm{m}}^{(3)}$ is decreased by the volume factor p_{m}, while $\chi_{\mathrm{m}}^{(3)}$ may be enhanced by local fields if $\mathrm{Re}(\varepsilon_{\mathrm{m}} + 2\varepsilon_{\mathrm{h}}) \approx 0$, which determines the resonance wavelength. In agreement with this model, an Au-dispersed glass, for instance, gives a greater $\chi^{(3)}$ than that of an Au film [44.5].

However, since these systems are complex, consisting of particles and a glass matrix, a variety of situations arise. For the particle, as well as particle species, we need to consider size, size distribution, shape and concentration. Here, needless to say, a narrow size distribution is preferred for investigating fundamental mechanisms. The shape may be spherical, ellipsoidal, rod, and so forth. The concentration determines the mean separation distance between particles. As the concentration increases, electrical particle–particle interactions appear [44.59], and then the particles eventually percolate [44.60], which may produce dramatic changes in the nonlinear response. The matrix seems to be of secondary importance. Actually, liquids and organic materials have been employed as well as glasses [44.4]. However, some reports suggest that the nonlinearity is greatly affected by the surface states of the semiconductor particles [44.72] and by the dielectric constant of the matrix surrounding the metallic particles [44.4].

Lastly, it may be worth mentioning two recent results. One is that particles can be arrayed to produce photonic structures that exhibit novel nonlinear properties, such as light confinement [44.73]. The other is the generation of second harmonic signals from oriented ellipsoidal Ag nanoparticles [44.74]. Oriented particle structures have been produced in silica through tensile deformation and simultaneous heating, and this may be regarded as a kind of mechanical poling.

44.4 Photoinduced Phenomena

The intense pulsed light employed to produce nonlinear effects is also likely to produce a variety of transitory and (quasi-)stable optical changes [44.72,75]. Photochromic effects induced by sub-gap light are the result of transitory electronic changes [44.76]. The increase in the refractive index of SiO_2 induced by fs–ns laser light with $\hbar\omega \approx 1 \approx 5$ eV is known to occur along with quasi-stable structural changes [44.11, 77]. The optical poling described in Sect. 44.2 can be regarded as a kind of photoinduced anisotropy. When the light is more intense than 1 GW/cm^2–1 TW/cm^2, depending on the duration of the light pulse, permanent damage is likely to occur [44.5]. These photosensitive changes are induced by electronic excitations, which may be triggered by one-photon and multiphoton processes, depending upon the photon energy and the light intensity.

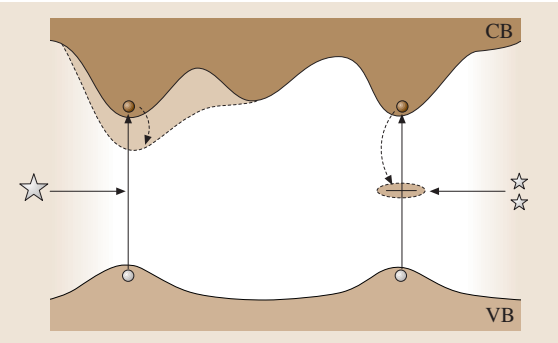

Fig. 44.7 Different relaxation paths from bandgap excitation due to one-photon (*left*) and two-photon (*right*) processes. For instance, the one-photon and two-photon excitations induce bonding strains and defect alterations

Are these photoinduced phenomena really excited by nonlinear processes? For instance, when a photoinduced phenomenon is induced by exposure to light of photonic energy $\hbar\omega \approx E_{\mathrm{g}}/m$, where m is an integer, it is often asserted that m-photon absorption is responsible. Nevertheless, the phenomenon may be triggered by one-photon absorption by mid-gap states, which give weak absorption tails (Fig. 44.2) arising from defective structures in the glass [44.25, 78]. Otherwise, it may be triggered by m-step absorption processes [44.79], consisting of m one-photon absorptions in succession (Fig. 44.1c). These processes have probably been overlooked when analyzing experimental results.

In addition, as schematically illustrated in Fig. 44.7, the structural changes induced by linear and nonlinear excitation are not necessarily the same. *Tanaka* has demonstrated using As_2S_3 that the bandgap excitations produced by one-photon and two-photon absorption produce different changes [44.78]. One-photon excitation leads to photodarkening, while two-photon excitation results in an increase in the refractive index with no photodarkening. In these phenomena, temperature rises upon intense exposure can be neglected. Such changes related to excitation processes can appear in glasses because the *localized* atomic wavefunction plays an important role, in contrast to the extended Bloch wavefunctions in crystals. For instance, as we can see from (44.4), one-photon excitation occurs between wavefunctions with different parities, such as from s to p orbitals, since H is an odd function. In contrast, (44.5) shows that two-photon excitation can occur between states of the same parity states, such as from p to p. In addition, the $1/(E_{ni} - \hbar\omega)$ in the equation leads to the possibility of *resonant and localized* two-photon excitation if $E_{ni} - \hbar\omega \approx 0$ is satisfied for a mid-gap state. In such cases, the mid-gap state selectively absorbs the excitation energy, leading to an atomic change which shows itself as a macroscopic photoinduced phenomenon.

44.5 Summary

At present, there is a big gap between the science and the technology of glasses. From a physical point of view, glass science lags far behind crystal science, mainly due to experimental difficulties associated with atomic structure determination and the theoretical unavailability of Bloch-type wavefunctions. On the other hand, it is now difficult to imagine a world without optical fibers. These contrasting situations are promoting a deeper understanding of nonlinear photonic glasses and are leading to an increasingly wide range of applications for such glasses.

Third-order optical nonlinearity in homogeneous glasses has been studied in a fair amount of detail. Substantial experimental data have been obtained for n_2, which have been analyzed using empirical relations such as those from Boling. In contrast, less work has been done on the nonlinear absorption β. In the present article, therefore, we have tried to present, in a coherent way, the absorption and the refractive index using semiconductor terminology. This approach can be used to connect nonlinear properties to the energy gap. However, little work has been done on the dynamics associated with this field. For instance, it is difficult to theoretically predict the response time τ in a glass at a particular excitation energy.

Two inhomogeneous systems have aroused increasing interest. One is poled or crystallized glass. Enhanced second-order nonlinearity has been reported for such systems, and this can sometimes be added selectively to a region. The other is the particle-embedded system, which can give greater third-order nonlinearity, and in some cases enhanced second-order nonlinearity too. However, the mechanism associated with this system remains to be studied. One experimental problem is to find a method that can reproduce particles of a fixed size and shape in arbitrary concentrations. These two inhomogeneous systems can be combined using photonic structure concepts, which will be of interest for future applications.

Finally, nonlinear optical excitations appear to play important roles in a variety of photoinduced phenomena in glasses. However, fundamental studies are still lacking in this area. The phenomenon of interest may be nonlinear in nature, or the linear excitation of gap states may trigger successive changes. Attempting to understand the nonlinear photo–electro–structural process will provide a challenging problem.

References

44.1 G. P. Agrawal: *Nonlinear Fiber Optics*, 3rd edn. (Academic, San Diego 2001)
44.2 P. P. Mitra, J. B. Stark: Nature **441**, 1027 (2001)
44.3 L. F. Mollenauer: Science **302**, 996 (2003)
44.4 R. L. Sutherland: *Handbook of Nonlinear Optics*, 2nd edn. (Marcel Dekker, New York 2003)
44.5 R. W. Boyd: *Nonlinear Optics*, 2nd edn. (Academic, San Diego 2003)

44.6 M. H. Field, J. Popp, R. K. Chang: *Progress in Optics Vol. 41*, ed. by E. Wolf (North Holland, Amsterdam 2000) Chap. 1
44.7 S. M. Spillane, T. J. Kippenberg, K. J. Vahala: Nature **415**, 621 (2002)
44.8 Y. Quiquempois, P. Niay, M. Dounay, B. Poumellec: Curr. Opinion Solid State Mater. Sci. **7**, 89 (2003)
44.9 U. Österberg, W. Margulis: Opt. Lett. **11**, 516 (1986)
44.10 A. Jha, X. Liu, A. K. Kar, H. T. Bookey: Curr. Opinion Solid State Mater. Sci. **5**, 475 (2001)
44.11 G. Pacchioni, L. Skuja, D. L. Griscom: *Defects in* SiO_2 *and Related Dielectrics: Science and Technology* (Kluwer, Dortrecht 2000)
44.12 E. M. Vogel, M. J. Weber, D. M. Krol: Phys. Chem. Glasses **32**, 231 (1991)
44.13 K. Tanaka: J. Mater. Sci: Mater Electron. **16**, 633 (2005)
44.14 M. E. Lines: J. Appl. Phys. **69**, 6876 (1991)
44.15 A. Zakery, S. R. Elliott: J. Non-Cryst. Solids. **330**, 1 (2003)
44.16 K. Tanaka: J. Non-Cryst. Solids. **338–340**, 534 (2004)
44.17 T. Mizunami, K. Takagi: Opt. Lett. **19**, 463 (1994)
44.18 A. Dragonmir, J. G. McInerney, N. Nikogosyan: Appl. Opt. **41**, 4365 (2002)
44.19 K. Tanaka, N. Yamada, M. Oto: Appl. Phys. Lett. **83**, 3012 (2003)
44.20 K. Tanaka: Appl. Phys. Lett. **80**, 177 (2002)
44.21 K. Ogusu, J. Yamasaki, S. Maeda, M. Kitao, M. Minakata: Opt. Lett. **29**, 265 (2004)
44.22 K. Imanishi, Y. Watanabe, T. Watanabe, T. Tsuchiya: J. Non-Cryst. Solids **259**, 139 (1999)
44.23 R. C. Enck: Phys. Rev. Lett. **31**, 220 (1973)
44.24 P. S. Weitzman, U. Osterberg: J. Appl. Phys. **79**, 8648 (1996)
44.25 S. R. Elliott: *Physics of Amorphous Materials*, 2nd edn. (Longman Scientific, Essex 1990)
44.26 N. Sugimoto, H. Kanbara, S. Fujiwara, K. Tanaka, K. Hirao: Opt. Lett. **21**, 1637 (1996)
44.27 S. Smolorz, I. Kang, F. Wise, B. G. Aiken, N. F. Borrelli: J. Non-Cryst. Solids **256 and 257**, 310 (1999)
44.28 O. Sugimoto, H. Nasu, J. Matsuoka, K. Kamiya: J. Non-Cryst. Solids. **161**, 118 (1993)
44.29 N. L. Boling, A. J. Glass, A. Owyoung: IEEE Quant. Electron. **14**, 601 (1978)
44.30 V. Dimitrov, S. Sakka: J. Appl. Phys. **79**, 1741 (1996)
44.31 J. Qi and D. F. Xue, G. L. Ning: Phys. Chem. Glasses **45**, 362 (2004)
44.32 S. Suehara, P. Thomas andA. Mirgorodsky, T. Merle-Mejean, J. C. Champarnaud-Mesjard, T. Aizawa, S. Hishita, S. Todoroki, T. Konishi, S. Inoue: J. Non-Cryst. Solids **345&346**, 730 (2004)
44.33 M. Sheik-Bahae, D. J. Hagan, E. W. Van Stryland: Phys. Rev. Lett. **65**, 96 (1990)
44.34 T. S. Moss: *Optical Properties of Semiconductors* (Butterworths, London 1959) p. 48
44.35 D. C. Hutchings, M. Sheik-Bahae, D. J. Hagan, E. W. Van Stryland: Opt. Quantum. Electron. **24**, 1 (1992)
44.36 M. Sheik-Bahae, D. C. Hutchings, D. J. Hagan, E. W. Van Stryland: IEEE Quantum Electron. **27**, 1296 (1991)
44.37 K. Tanaka: *Optoelectronic Materials and Devices*, Vol. 1, ed. by G. Lucovsky, M. Popescu (INOE, Bucharest 2004) Chap. 3
44.38 J. Bromage: J. Lightwave Technol. **22**, 79 (2004)
44.39 A. Zheltikov: Appl. Phys. B **77**, 143 (2003)
44.40 V. Mizrahi, K. W. DeLong, G. I. Stegeman, M. A. Saifi, M. J. Andrejco: Opt. Lett. **14**, 1140 (1989)
44.41 M. Asobe: Opt. Fiber Technol. **3**, 142 (1997)
44.42 G. I. Stegeman, R. H. Stolen: J. Opt. Soc. Am. B **6**, 652 (1989)
44.43 K. Tanaka, T. Gotoh, N. Yoshida, S. Nonomura: J. Appl. Phys. **91**, 125 (2002)
44.44 A. K. Abeeluck, C. Headley: Appl. Phys. Lett. **85**, 4863 (2004)
44.45 H.-Y. Chen, C.-L. Lin, Y.-H. Yang, S. Chao, H. Niu, C. T. Shih: Appl. Phys. Lett. **86**, 81107 (2005)
44.46 R. H. Stolen, H. W. K. Tom: Opt. Lett. **12**, 585 (1987)
44.47 R. A. Myers, N. Mukherjee, S. R. J. Brueck: Opt. Lett. **22**, 1732 (1991)
44.48 Y. Luo, A. Biswas, A. Frauenglass, S. R. Brueck: Appl. Phys. Lett. **84**, 4935 (2004)
44.49 B. Ferreira, E. Fargin, J. P. Manaud, G. Le Flem, V. Rodriguez, T. Buffeteau: J. Non-Cryst. Solids **343**, 121 (2004)
44.50 G. S. Murugan, T. Suzuki, Y. Ohishi, Y. Takahashi, Y. Benino, T. Fujiwara, T. Komatsu: Appl. Phys. Lett. **85**, 3405 (2004)
44.51 A. Okada, K. Ishii, K. Mito, K. Sasaki: Appl. Phys. Lett. **60**, 2853 (1992)
44.52 P. G. Kazansky, A. Kamal, P. St. Russell: Opt. Lett. **18**, 683 (1993)
44.53 Q. M. Liu, F. X. Gan, X. J. Zhao, K. Tanaka, A. Narazaki, K. Hirao: Opt. Lett. **26**, 1347 (2001)
44.54 L. J. Henry, B. V. McGrath, T. G. Alley, J. J. Kester: J. Opt. Soc. Am. B **13**, 827 (1996)
44.55 O. Deparis, C. Corbari, G. Kazansky, K. Sakaguchi: Appl. Phys. Lett. **84**, 4857 (2004)
44.56 V. Pruneri, P. G. Kazansky, D. Hewak, J. Wang, H. Takebe, D. N. Payne: Appl. Phys. Lett. **70**, 155 (1997)
44.57 Y. Takahashi, Y. Benino, T. Fujiwara, T. Komatsu: Appl. Phys. Lett. **81**, 223 (2002)
44.58 R. T. Hart, K. M. Ok, P. S. Halasyamani, J. W. Zwanziger: Appl. Phys. Lett. **85**, 938 (2004)
44.59 Y. Hamanaka, K. Fukuta, A. Nakamura, L. M. Liz-Marzan, P. Mulvaney: Appl. Phys. Lett. **84**, 4938 (2004)
44.60 R. Del Coso, J. Requejo-Isidro, J. Solis, J. Gonzalo, C. N. Afonso: J. Appl. Phys. **95**, 2755 (2004)
44.61 Q. F. Zhang, W. M. Liu, Z. Q. Xue, J. L. Wu, S. F. Wang, D. L. Wang, Q. H. Gong: Appl. Phys. Lett. **82**, 958 (2003)
44.62 W. Wang, G. Yang, Z. Chen, Y. Zhou, H. Lu, G. Yang: J. Appl. Phys. **92**, 7242 (2002)

44.63 A. Clementi, N. Chiodini, A. Paleari: Appl. Phys. Lett. **84**, 960 (2004)
44.64 S. G. Lu, Y. J. Yu, C. L. Mak, K. H. Wong, L. Y. Zhang, X. Yao: Microelectronic Eng. **66**, 171 (2003)
44.65 F. Gonella, P. Mazzoldi: *Handbook of Nanostructured Materials and Nanotechnology*, Vol. 4, ed. by H. S. Nalwa (Academic, San Diego 2000) Chap. 2
44.66 V. M. Shalaev: *Nonlinear Optics of Random Media* (Springer, Berlin, Heidelberg 2000)
44.67 G. Banfi, V. Degiorgio, D. Ricard: Adv. Phys. **47**, 510 (1998)
44.68 M. Nogami, S. T. Selvan, H. Song: Photonic glasses: Nonlinear optical and spectral hole burning properties. In: *Handbook of Advanced Electronic and Photonic Materials and Devices*, Vol. 5, ed. by H. S. Nalwa (Academic, San Diego 2001) Chap. 5
44.69 J. He, W. Ji, G. H. Ma, S. H. Tang, H. I. Elim, W. X. Sun, Z. H. Zhang, W. S. Chin: J. Appl. Phys. **95**, 6381 (2004)
44.70 Y. Li, M. Takata, A. Nakamura: Phys. Rev. B **57**, 9193 (1998)
44.71 D. Stroud, P. M. Hui: Phys. Rev. B **37**, 8719 (1988)
44.72 A. Puzder, A. J. Williamson, F. Gygi, G. Galli: Phys. Rev. Lett. **92**, 217401 (2004)
44.73 M. Ajgaonkar, Y. Zhang, H. Grebel, C. W. White: Appl. Phys. Lett. **75**, 1532 (1999)
44.74 A. Podlipensky, J. Lange, G. Seifert, H. Graener, I. Cravetchi: Opt. Lett. **28**, 716 (2003)
44.75 R. C. Jin, Y. C. Cao, E. C. Hao, G. S. Metraux, G. C. Schatz, C. A. Mirkin: Nature **425**, 487 (2003)
44.76 Y. Watanabe, Y. Kikuchi, K. Imanishi, T. Tsuchiya: Mater. Sci. Eng. B **54**, 11 (1998)
44.77 J. S. Aitchison, J. D. Prohaska, E. M. Vogel: Met. Mater. Proc. **8**, 277 (1996)
44.78 K. Tanaka: Philos. Mag. Lett. **84**, 601 (2004)
44.79 K. Kajihara, Y. Ikuta, M. Hirano, H. Hosono: Appl. Phys. Lett. **81**, 3164 (2002)